ChemCatChem

Research Article
doi.org/10.1002/cctc.202300078

Chemistry Europe
European Chemical Societies Publishing

www.chemcatchem.org

Special Collection

Plasma-catalytic Ammonia Synthesis via Eley-Rideal Reactions: A Kinetic Analysis

Kevin H. R. Rouwenhorstm[a, b, c] and Leon Lefferts*[a]

The reaction mechanism of plasma-catalytic ammonia synthesis is not fully understood. MgO supported Ru, Co, Pt, Pd, Cu and Ag catalysts are tested in a DBD plasma at temperature between room temperature and 500 °C and plasma power between 3.8 W and 6.4 W. The resulting ammonia production in the presence of a plasma and a catalyst can be distinguished into (1) temperature-independent plasma-based ammonia synthesis, and (2) temperature-dependent plasma-catalytic ammonia synthesis. Turn-over-frequencies (TOF) are calculated based on the rate of the second pathway and chemisorption data, measuring the number of active sites. Underestimation of TOFs caused by ammonia decomposition was minimized by using exclusively observations at low ammonia concentration. The kinetic results suggest that the Eley-Rideal reaction between N radicals from the plasma with chemisorbed H atoms is the rate-determining step for plasma-catalytic ammonia synthesis on Ru/MgO, Co/MgO, Pt/MgO, Pd/MgO, and Cu/MgO, with apparent activation barriers in the range 18–24 kJ mol^{-1}. In contrast, the apparent activation barrier on Ag/MgO is significant higher at 30 kJ mol^{-1}, suggesting a shift in rate determining step. The low H coverage on Ag may induce a shift to a Langmuir-Hinshelwood pathway, via adsorption of N radicals on the metal surface.

Introduction

Renewable energy sources increasingly penetrate the electricity grid, spurring the electrification of the energy landscape.[1] Plasma-activation of chemical bonds is one of the alternatives considered for electrified chemical processes, next to electrochemical processes.[2–4] Plasma-reactions merit from fast response to intermittent electricity, and this potentially allows processes to operate under mild conditions.[2–5] The introduction of a catalyst in a plasma-driven process may allow for selective production of the desired product.[4] However, the fundamentals of the mutual plasma-catalyst influences are not fully understood.[6,7]

[a] Dr. K. H. R. Rouwenhorstm, Prof. Dr.Ir. L. Lefferts
Catalytic Processes & Materials
MESA + Institute for Nanotechnology
University of Twente
P.O. Box 217, 7500 AE Enschede (The Netherlands)
E-mail: l.lefferts@utwente.nl
Homepage: https://www.utwente.nl/en/tnw/cpm/
[b] Dr. K. H. R. Rouwenhorstm
Proton Ventures
Karel Doormanweg 5
3115 Schiedam (The Netherlands)
[c] Dr. K. H. R. Rouwenhorstm
Ammonia Energy Association
77 Sands Street, 6th Floor
Brooklyn NY 11201 (USA)

Supporting information for this article is available on the WWW under https://doi.org/10.1002/cctc.202300078

This publication is part of a joint Special Collection with EurJOC and EurJIC on the Netherlands Institute for Catalysis Research. Please see our homepage for more articles in the collection.

Plasma-catalytic ammonia synthesis has gained traction as a model system for studying plasma catalysis due to the relative simplicity of the reaction in the absence of any by-products. Furthermore, ammonia is considered as a zero-carbon fuel and hydrogen carrier in a hydrogen economy.[8–11] Various authors have reviewed plasma-catalytic ammonia synthesis.[12–16]

The mechanism of plasma-catalytic ammonia synthesis is not fully understood,[17] and various schemes have been proposed. Mehta et al.[18,19] proposed that plasma-catalytic ammonia synthesis occurs via vibrationally activated molecular N_2. The key assumption is that plasma-activation of N_2 decreases the barrier for N_2 dissociation on the catalyst surface. The subsequent hydrogenation reactions on the catalyst surface are not affected. The activity for ammonia synthesis on different metals varies by orders of magnitude, with a distinctive volcano curve similar to thermal catalysis.[18,20] However, the predicted volcano curve for plasma-catalysis with plasma-activated N_2 shifts towards more noble metals. Previously, we showed that at relatively low specific energy inputs (SEIs) of 0.1–0.4 kJ L^{-1}, molecular plasma-activated N_2 is the dominant species for NH_3 synthesis on Ru-catalysts in the temperature range 200–300 °C.[21,22]

Chen et al.,[23] Engelmann et al.,[24] Gorbanev et al.,[25] Rouwenhorst et al.,[26] Shah et al.,[27] and Yamijala et al.[28] proposed that plasma-catalytic ammonia synthesis proceeds via N and NH_X radicals, especially at high plasma powers. The dominant contribution of radical species was demonstrated by various authors for SEIs in the range of 10 to 19 kJ L^{-1} on Ru-catalysts,[29], and at 40 kJ L^{-1} on Fe-, Ru-, Co-, and Cu-catalysts.[25] Ammonia synthesis may occur via radical adsorption with subsequent surface reactions, i.e. Langmuir-Hinshelwood reactions. Alternatively, plasma radicals may directly interact with surface-adsorbed species and react to form ammonia via Eley-Rideal reactions. Engelmann et al.[30] performed density func-

tional theory (DFT) calculations, predicting that adsorption of plasma radicals with subsequent Langmuir-Hinshelwood hydrogenation reactions results in significant difference in activity among transition metals for plasma-catalytic ammonia synthesis, varying by orders of magnitude. Eley-Rideal reactions would result in similar activities among transition metals.[30]

Various authors have experimentally investigated the plasma-catalytic activity on transition metals in dielectric barrier discharge (DBD) reactors.[18,31–37] Unfortunately, all these studies have not considered at least one of the following four complications: (1) sufficiently broad selection of metals, (2) rigorous characterization of the number of metal surface atoms with appropriate techniques, (3) minimizing the metal loading to minimize influencing the plasma, and (4) minimizing the ammonia concentration to minimize ammonia decomposition at constant specific energy input. Plasma-induced ammonia decomposition would cause underestimation of the plasma-catalytic activity. Furthermore, the temperature was constant in most studies, not allowing for a kinetic analysis.

The current work considers all these complications, by assessing the activity for plasma-catalytic ammonia synthesis of Ru/MgO, Co/MgO, Pt/MgO, Pd/MgO, Cu/MgO, and Ag/MgO catalysts with low metal loading (2 wt.%) in a DBD reactor operated with SEIs in the range of 10 to 19 kJ L^{-1}. The catalyst have been characterized with both chemisorption and XRD. Furthermore, the NH_3 concentration is kept relatively mild low ($<$ 0.5 mol. %), suppressing plasma-driven ammonia decomposition. We distinguish between plasma chemistry contributions and plasma-catalytic effects and temperature is varied, allowing for a kinetic analysis.

Results & discussion

The conversion to ammonia with bare MgO in the presence of plasma is measured in the DBD reactor, described in the Experimental Section, to benchmark the conversion to ammonia with the MgO-supported metal catalysts. As shown in Figure 1, the conversion on bare MgO is independent of temperature. Clearly, these reactions are not thermally activated. We attribute this conversion in absence of any metal catalyst to radical reactions in the plasma or reactions on the oxide surface, e.g. between N, H, and N_YH_X species.[38]

The synthesized catalysts (Ru/MgO, Co/MgO, Pt/MgO, Pd/MgO, Cu/MgO and Ag/MgO) contain about 2 wt% metal according to XRF analysis (Table S1). The metal dispersion according to XRD line broadening and chemisorption can be found in section S2.3. Catalysts are reduced at 500 °C in the reactor for 2 h in 20% H_2 (balance N_2) before the experiment started. Importantly, all results reported in Figure 1 are obtained operating with 3.8 W plasma power.

The conversion at room temperature on all catalysts is identical to the conversion on exclusively MgO at room temperature. This implies that the presence of metal nanoparticles with a relatively low loading (2 wt. %) does not significantly influence the plasma chemistry, which is in line with literature for low metal loadings.[36,39] This is further supported by the fact that the Lissajous plots for MgO and Ru/MgO measured at room temperature are very similar (Figure S2). However, the conversion over the catalysts increases with increasing temperature, typical for a catalytic reaction.[29]

All catalysts were tested for thermal-catalytic ammonia synthesis in absence of plasma. The thermal-catalytic activity of all catalysts is too low to detect any ammonia with the equipment used under the experimental conditions in this study. Therefore, the difference between the ammonia concentration due to plasma chemical reactions, as observed with MgO, and the ammonia concentration observed with supported-metal catalysts is a measure for the rate of plasma-catalytic ammonia formation.

Ammonia is synthesized beyond thermal equilibrium for all catalysts at temperatures above 400 °C (Figure 1), in line with results reported in literature.[29,40] Apparently, plasma-catalytic ammonia synthesis is faster than the combination of thermal-catalytic ammonia decomposition and plasma induced ammonia decomposition. Exclusively Ru/MgO shows a decrease in ammonia outlet concentration upon increasing the temperature above 400 °C (Figure 1). Ru is known to be the most active catalyst for thermal-catalytic ammonia decomposition,[41,42] and this is confirmed in an experiment with co-feeding ammonia in absence of plasma (Figure S7), showing ammonia conversion at temperatures above 400 °C. All other catalysts are not significantly active at temperatures up to 500 °C (not shown).

Plasma-catalytic ammonia synthesis activity

The ammonia synthesis rate can be obtained via Equation 1, where $r_{M/MgO}$ is the total ammonia synthesis rate in the reactor (mmol-NH_3 min^{-1}), x_{NH3} the outlet NH_3 concentration (mol. fraction) and F_{gas} the inlet gas flow rate (20 mL min^{-1}). The correction factor 0.043 kmol-NH_3 m^{-3} accounts for the molar gas density of ammonia, e.g. the density of an ideal gas at NTP (Eq. 1).

$$r_{M/MgO} = 0.043 \cdot F_{gas} \cdot x_{NH_3} \quad (1)$$

The plasma-catalytic ammonia synthesis rate is calculated by subtracting the rate of plasma-chemical ammonia synthesis on MgO (r_{MgO} in mol min^{-1}) from the total ammonia synthesis rate in the reactor ($r_{M/MgO}$ in mol min^{-1}). The TOF, which is the number of molecules ammonia produced on one surface metal atom (s^{-1}) is calculated according to Equation 2. W_{cat} is the amount of catalyst in the reactor (g), [M] is the metal loading of the catalysts (wt. fraction, Table S1), d is the dispersion (fraction of metal atoms at the surface, Table S1), and A_M is the atomic weight of the metal.

$$TOF = \frac{\left(r_{\frac{M}{MgO}}\right) - r_{MgO}) \cdot A_M}{60 \cdot W_{cat} \cdot [M] \cdot d} \quad (2)$$

As discussed in supporting information section S3.2, the ammonia outlet concentration must be below 0.7 mol. % and plasma powers should be limited to 3.8 W to minimize the rate

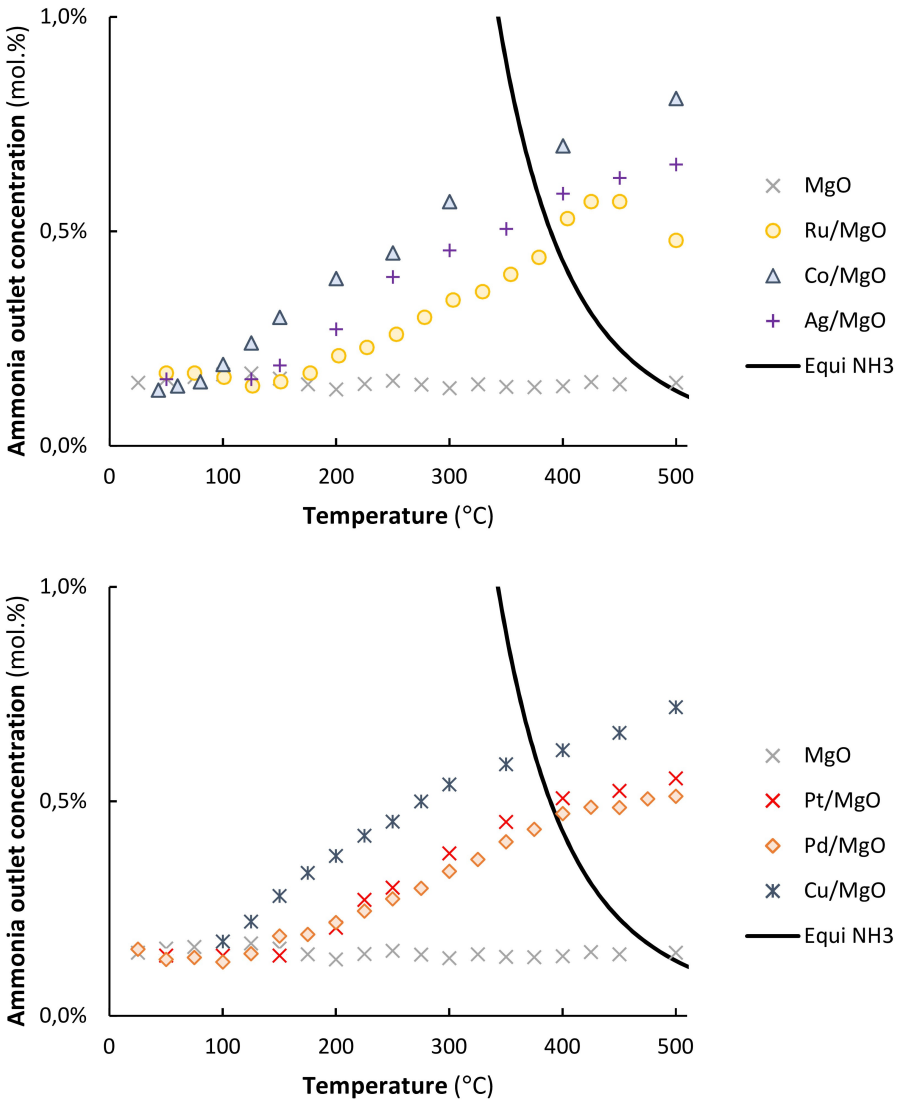

Figure 1. Activity for plasma-chemical NH_3 synthesis and plasma-catalytic NH_3 synthesis (and decomposition) for MgO (× grey crosses), Ru/MgO (○ yellow circles), Co/MgO (△ blue triangles), Pt/MgO (× red crosses), Pd/MgO (◇ orange diamonds), Cu/MgO (✳ blue stars), and Ag/MgO (+ purple plusses) as function of temperature. Total flowrate 20 mL min^{-1}, atmospheric pressure, H_2:N_2 = 1:1 (no NH_3 co-feed), catalyst loading 130–150 mg (250–300 µm particles), plasma power 3.8 W (SEI = 11.4 kJ L^{-1}). The line labelled 'Equi NH3' is the thermodynamic equilibrium for a 1:1 H_2:N_2 ratio as calculated using the SRK property package in Aspen Plus.

of ammonia decomposition. If these criteria are met, the plasma-catalytic ammonia synthesis rate can be calculated using Equation 2. The Arrhenius plots for the different catalysts at ammonia outlet concentrations below 0.5 mol.% and at a plasma power of 3.8 W is shown in Figure 2.

The resulting apparent activation barriers for plasma-catalytic ammonia synthesis on the different metals are in the range 18–24 kJ mol^{-1} (see Figure 2b), except for Ag/MgO showing a higher apparent barrier of 30 kJ mol^{-1}.

Reaction mechanism

All transition metals show an activity within the same order of magnitude, with a turnover frequency in the order of 10^{-3}–10^{-2} s^{-1} at 250 °C (see Figure 3). The similar activity among transition metals is in accordance with previous literature under similar plasma conditions and at similar temperatures.[18,37]

It should be noted that the reported turnover frequencies obtained in this work, e.g. in the order 10^{-3}–10^{-2} s^{-1} are lower than results obtained from microkinetic modelling calculations, which predict activities up to 10^{1} s^{-1} for a uniform plasma, 10^{0} s^{-1} for microdischarges, and 10^{-2} s^{-1} for the filamentary afterglow.[30] This discrepancy may be attributed to the fact that exclusively the external surface of the catalyst is exposed to the plasma. Most active sites are located at the internal surface of the catalyst, e.g. not in direct contact with the plasma.[12,17] Thus, the actual plasma-catalytic activity at the external surface is underestimated. A possible solution for future research is to use dense catalyst materials with active metals only exposed at

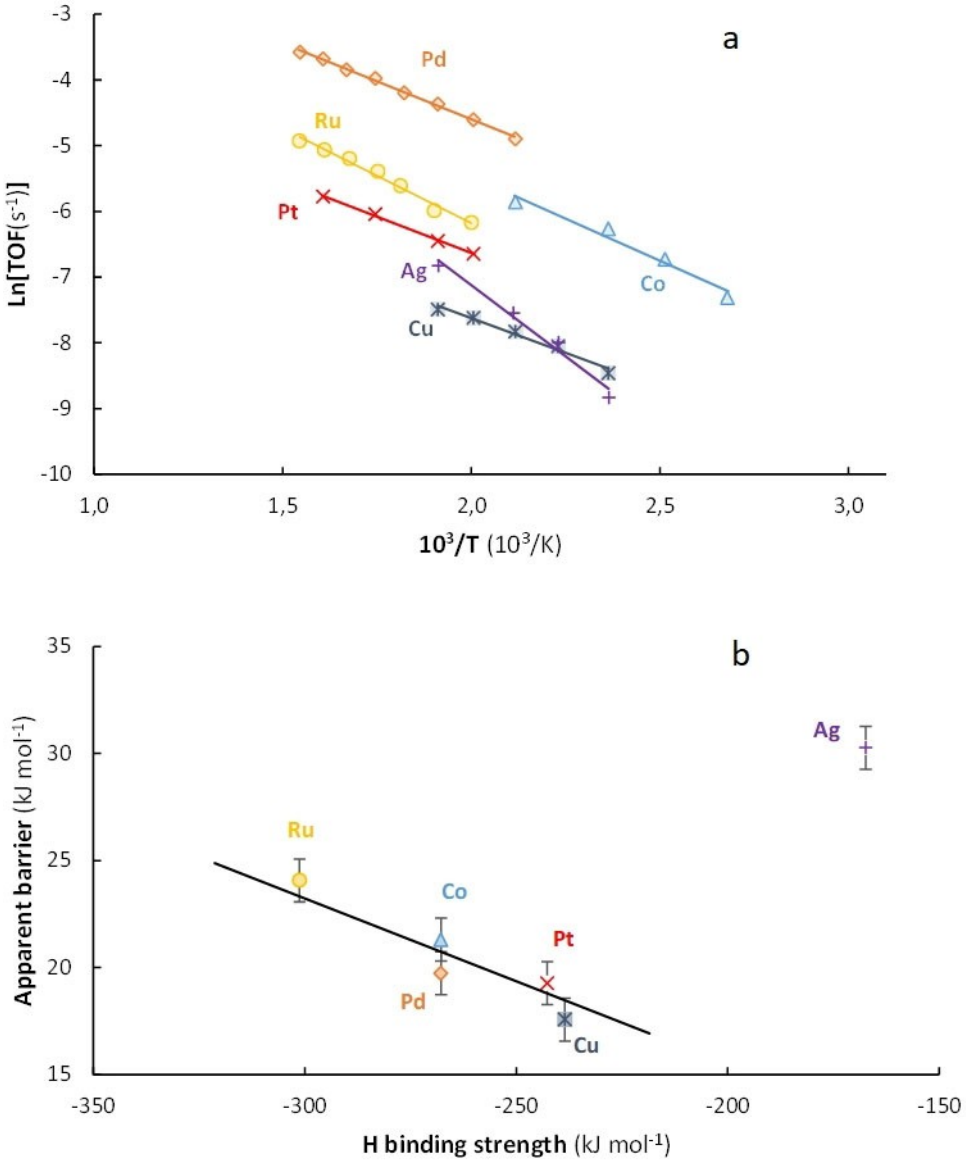

Figure 2. a.) Arrhenius plots for plasma-catalytic NH_3 synthesis on Ru/MgO (○ yellow circles), Co/MgO (△ blue triangles), Pt/MgO (× red crosses), Pd/MgO (◇ orange diamonds), Cu/MgO (⁎ blue stars) and Ag/MgO (+ purple plusses). b.) Apparent activation barriers for plasma-catalytic ammonia synthesis for various metals versus the H binding energy. Catalysts: Ru/MgO (○ yellow circles), Co/MgO (△ blue triangles), Pt/MgO (× red crosses), Pd/MgO (◇ orange diamonds), Cu/MgO (⁎ blue stars) and Ag/MgO (+ purple plusses). The obtained values are valid for an ammonia outlet concentration below 0.5 mol.% NH_3, SEI = 11 kJ L^{-1}, flow rate 20 mL min^{-1}, H_2:N_2 = 1:1. H binding strengths are based on.[43]

the external catalyst surface, such that the calculated TOF is in line with the exposed external surface.

Several observation support the hypothesis that a reaction pathway via N radicals in the plasma is dominant. Firstly, ammonia is formed in presence of plasma and bare MgO (see Figure 1), e.g. without a catalyst that would be able to dissociate the N_2 molecule, clearly indicating that N_2 dissociation occurs in the plasma. Secondly, we observe that increasing SEI causes both increasing conversion (Figure S10), and increasing concentration of excited N_2 molecules, as observed with UV-Vis spectroscopy (Figure S4). Plasma modelling results show that, under the conditions applied (Supporting information section S2.5), both the concentrations of electronically excited N_2, as observed, and the concentration of N radicals increase with an increasing reduced electrical field and with increasing SEI. In short, the high ammonia formation rate in case of high concentration of N radicals suggest formation of ammonia via N radicals. The same qualitative argument can be made on increasing the N_2 concentration, causing increasing conversion (Figure S11), and increasing N_2 activation (Figure S5).

The activity of different metals would change by orders of magnitude if molecular plasma-activated N_2 would be dominant, as part of the N_2 dissociation would still occur on the catalyst, e.g. an activated process varying strongly between metals.[18,30] Previous modelling work of Engelmann et al.[30] suggests that a kinetic model involving N radicals and just

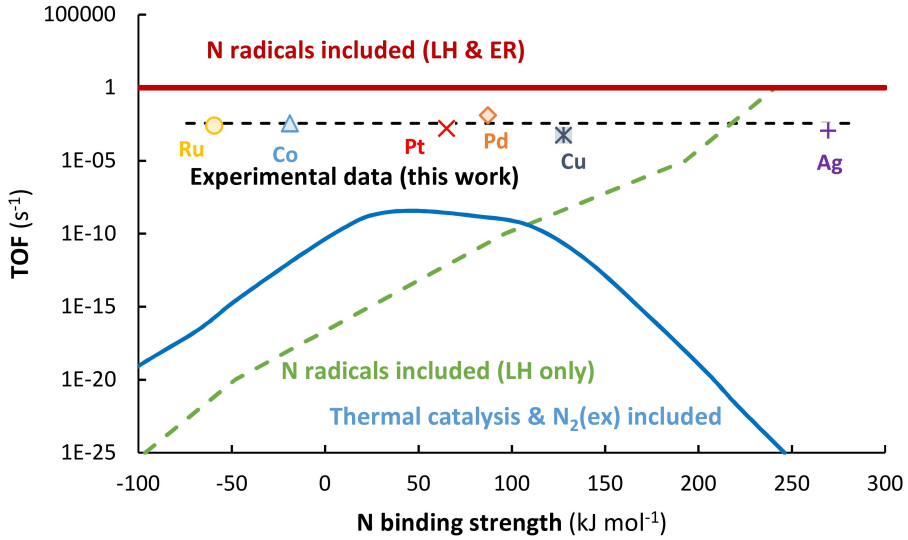

Figure 3. Turnover frequencies (TOFs) calculated in this work (black dotted line, various symbols), compared to microkinetic model predicts of Engelmann et al.[30] at $H_2:N_2 = 3:1$, 400 K during micro-discharge. LH: Langmuir-Hinshelwood. ER: Eley-Rideal.

Langmuir-Hinshelwood surface reactions would still result in multiple orders of magnitude activity difference among metals (see Figure 3). Furthermore, the barriers of 18–24 kJ mol^{-1} for plasma-catalytic ammonia synthesis on Ru, Co, Pt, Pd, and Cu (Figure 4) are too low for N_2 dissociation (> 50 kJ mol^{-1}), and too low for NH_X hydrogenation reactions on the metal surface (50–150 kJ mol^{-1}), as follows from density functional theory (DFT) calculations.[44,45]

Additionally, the modelling work of Engelmann et al.[30] suggests that the similar activity among metals can only be explained by an Eley-Rideal reaction as rate-determining step, rather than a Langmuir-Hinshelwood surface reaction. Thus, the similar activity among metals within the same order of magnitude suggest that N radicals are the dominant reactant nitrogen species for plasma-catalytic ammonia synthesis at relatively high plasma powers (≥1 kJ L^{-1}), as opposed to molecular plasma-activated N_2.

In our previous work with Ru catalysts and similar SEI values between 10 and 19 kJ L^{-1}, we demonstrated that N radicals are indeed the dominant nitrogen species for plasma-catalytic ammonia synthesis, at temperatures below 300 °C, where thermal-catalytic activity for N_2 dissociation is negligible.[29] The other metals tested in this work have an even higher barrier for N_2 dissociation as compared to Ru, implying that the role of N_2 dissociation will also be negligible for the other metals. Thus, ammonia formation via N radicals in the plasma is the dominant pathway, and N_2 dissociation on the metal surface does not play a significant role.

For all metals, except Ag, the activation barrier decreases with decreasing bonding strength of H to the metal surface. Figure 2b shows a strong correlation between the experimental

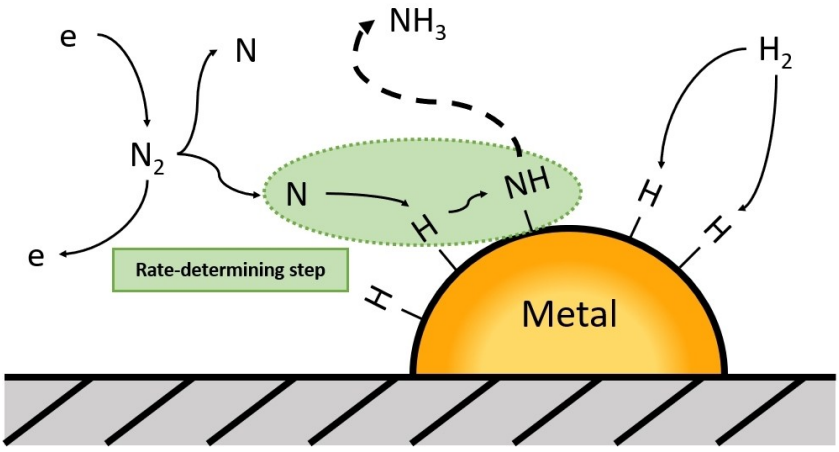

Figure 4. Schematic representation of the proposed rate-determining reaction step for all metals except for Ag, e. g. via the Eley-Rideal Reaction between a N radical from the plasma and surface-adsorbed H.

activation barriers and the H bonding strength on the different metals, suggesting that the rate-determining reaction step involves breaking the H-surface bond. We suggest that the reaction between a N radical from the plasma phase and adsorbed H is rate-limiting for plasma-catalytic ammonia synthesis on Ru, Co, Pt, Pd, and Cu at relatively high plasma powers ($\geq$ 1 kJ L^{-1}),[46] as schematically represented in Figure 4. This is consistent with recent modelling work of Engelmann et al.,[30] who assumed plasma properties similar to the current DBD reactor. Subsequent L–H type of hydrogenation steps to ammonia are expected to be fast, based on microkinetic modelling studies.[30,28]

The exception is Ag, one of the few metals that cannot thermally chemisorb H_2. Therefore, recombination of H-atoms to form gaseous H_2 is highly exothermic, causing low H coverage and significant energy dissipation. The resulting low H surface coverage decreases the contribution of the E–R pathway. The apparent activation barrier (30 kJ mol^{-1}) is much higher compared to all other metals (18–24 kJ mol^{-1}), supporting the suggestion that the rate determining step changes, probably as part of a L–H pathway.

Conclusion

Plasma-catalytic ammonia synthesis was studied for Ru/MgO, Co/MgO, Pt/MgO, Pd/MgO, Cu/MgO, and Ag/MgO. The temperature is varied between room temperature and 500 °C, and the plasma power is varied between 3.8 W and 6.4 W. TOFs for ammonia formation in the presence of plasma with constant power are calculated after correction for non-catalytic ammonia formation in the plasma and based on thorough determination of the number of active sites with chemisorption. Non-catalytic ammonia formation in plasma is not influenced by the low loading of metals, confirming that plasma chemistry is not influenced by the presence of the low metal loading. TOFs are calculated exclusively based on observations at low conversion, in order to minimize ammonia decomposition, which would cause underestimation of the rate of formation. Plasma-catalytic ammonia formation is temperature-dependent, and the kinetic analysis suggests that the reaction between N radicals from the plasma with surface-adsorbed H is the dominating rate-determining step for Ru/MgO, Co/MgO, Pt/MgO, Pd/MgO and Cu/MgO. This E–R mechanism is in good agreement with recent modelling results[24] and leads to apparent activation barriers in the range 18–24 kJ mol^{-1}. The apparent activation barrier of 30 kJ mol^{-1} on Ag/MgO for plasma-catalytic ammonia synthesis is significantly higher, indicating a shift in the rate limiting step or a change in the dominant pathway form E–R to L–H, caused by a low coverage of Ag with H.

Experimental Section

Reactor set-up

A schematic representation of the experimental set-up for the catalytic tests is shown in Figure 5. The catalytic tests were carried out in a quartz tubular reactor with an inner diameter of 4 mm and an outer diameter of 6 mm, at atmospheric pressure. A stainless-steel rod of 1 mm diameter is placed inside the reactor as the high voltage electrode. At the outside of the quartz tube, a metal tube is placed as the ground electrode. The temperature was controlled with a thermocouple connected to a tubular oven, which is placed around the ground electrode. The temperature is controlled with typically 3 °C variation. The flowrates of the reactants were controlled with calibrated mass flow controllers (MFCs). About 130–150 mg of catalyst with particle size 250–300 μm was loaded in the reactor, on top of a layer of quartz wool. A spacer is placed above the catalytic bed to prevent moving of particles due to plasma-ignition and to center the high voltage electrode.

Before the catalytic tests, the catalysts were reduced at 500 °C in the reactor for 2 h in a gas mixture of 40 mL min^{-1} N_2 and 10 mL min^{-1} H_2, e.g. to remove any moisture or oxygenates. Thereafter, the catalytic tests were performed under steady-state conditions, typically at a total flowrate of 20 mL min^{-1} and a H_2:N_2 ratio of 1:1. The product gases were analyzed using an on-line Pfeiffer Vacuum Thermostar™ gas analysis system, which is a mass spectrometer (MS). The MS signal for NH_3 (17 m/e) was calibrated in the range 0–2 mol.%, resulting in a linear relationship. The signals for H_2 (2 m/e), N_2 (28 m/e) and H_2O (18 m/e) were also monitored semi-quantitatively, as well as a minor NH_3 peak (16 m/e). The MS

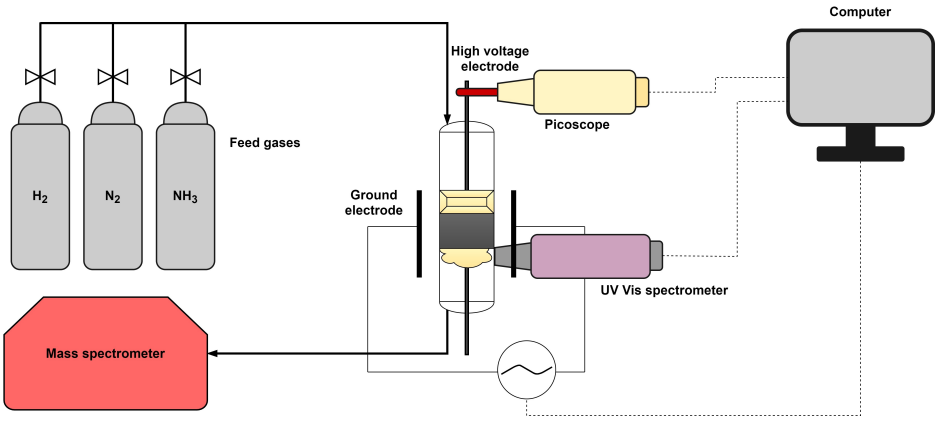

Figure 5. Schematic representation of the experimental set-up. The plasma volume includes the spacer on top of the bed, the packed bed, and the quartz wool. The oven around the plasma zone and the temperature control are not included because of clarity reasons.

signal at 17 m/e is not compromised by presence of any water, as shown in S6.

Plasma characterization

A PMV 500–4000 power supply was used to power the plasma at 25 kHz. A Picoscope PC Oscilloscope was used to monitor the charge-voltage characteristics. The high voltage electrode was connected to the power supply, and an AC voltage of up to 10 kV peak to peak was applied. A Tektronix P6015 A high voltage probe was used to monitor the voltage over the high voltage electrode, while a TT-HV 250 voltage probe was used to measure the voltage over the ground electrode. A capacitor of 8.24 nF was placed in between the ground electrode and the TT-HV 250 voltage probe. An Ocean HDX Spectrometer was used to analyse UV-Vis light emitted by the plasma at room temperature, just below the catalyst bed supported by the quartz wool. The camera of the spectrometer was screwed directly onto a hole in the outer electrode, allowing for measurements close to the plasma.

Materials

Cobalt(II) nitrate hexahydrate ($Co(NO_3)_2 \cdot 6H_2O$, 97.7% min), Palladium(II) nitrate hydrate ($Pd(NO_3)_2 \cdot xH_2O$, 99.8% Pd on metal basis), Tetraammineplatinum(II) nitrate ($Pt(NH_3)_4(NO_3)_2$) and Ruthenium(III) nitrosyl nitrate ($Ru(NO)(NO_3)_3$, >31.3 wt.% Ru) were purchased from Alfa Aesar. Copper(II) nitrate trihydrate ($Cu(NO_3)_2 \cdot 3H_2O$), and Silver nitrate ($AgNO_3$) were purchased from Merck.

Magnesium oxide powder (MgO, >97% purity grade) was purchased from Merck. H_2 and N_2 with a purity grade of 99.999% were purchased from Linde. Oxygen and water traces were removed using Agilent gas clean purification systems. A gas mixture of 2 vol.% NH_3 in a 98 vol.% N_2 balance gas was purchased from Linde. All materials were used as received. Deionized water was used during catalyst preparation.

Catalyst preparation

The metal precursors were dissolved in water and impregnated on the MgO support using the dry impregnation method.[47]. About 1.2 mL water was used per gram of MgO. Then, the mixture was dried in an oven at 105 °C and atmospheric pressure in air for 1 h, followed by drying in a vacuum oven at 120 °C for at least 2 h.

The dried catalysts were calcined in a calcination oven with 20 mL min^{-1} air flow at 400 °C for 2 h (heating rate 10 °C min^{-1}) decomposing the metal precursors. Subsequently, the metal oxides were reduced in a 20 mL min^{-1} H_2 flow at 550 °C for 2.5 h (heating rate 10 °C min^{-1}). After reduction, the catalysts were pelletized using a press and crushed. The sieve fraction 250–300 μm was used for the catalytic tests. Last traces of H_2O were removed in the reactor at 500 °C.

Catalyst characterization

The elemental composition was determined by x-ray fluorescence spectroscopy (XRF) using a Bruker S8 tiger. The total surface area and pore volume was determined by N_2 physisorption at −198 °C using a Micromeritics Tristar. The samples were outgassed in vacuum at 300 °C for 24 h before the analysis. The crystalline phases present in the catalysts were determined with X-ray diffraction (XRD) using a Bruker D2 Phaser diffractometer equipped with a position-sensitive detector over a 2θ range between 10° and 90° using Cu Kα radiation (λ = 1.5418 Å). The Scherrer equation was used to calculate the crystallite size of metal nanoparticles (Equation 3), where τ is the mean size of crystallites (nm), K is a dimensionless shape factor (0.9), λ is the x-ray wavelength, β is the line broadening at half of the maximum intensity (FWHM in radians), and θ is the Bragg angle.

$$\tau = \frac{\mathbf{K}\lambda}{\beta \mathbf{cos}(\theta)} \quad (3)$$

The total metal surface area was determined with H_2 chemisorption (Pt, Pd, Co), CO chemisorption (Ru) and N_2O chemisorption (Cu and Ag).

Supporting Information

The experimental set-up. The results of the catalyst characterization and plasma characterization with Lissajous plots and UV-Vis spectroscopy can be found in the supporting information. Additional plasma-catalytic experiments can also be found in the supporting information. Additional references cited within the Supporting Information.[48–54]

Author contributions

K. H. R. R. performed ammonia synthesis experiments. K. H. R. R. performed plasma characterization experiments. K. H. R. R. and L. L. co-wrote the manuscript. All authors discussed the results.

Acknowledgements

This project is co-financed by TKI-Energie from Toeslag voor Topconsortia voor Kennis en Innovatie (TKI) from the Ministry of Economic Affairs and Climate Policy, the Netherlands. The authors acknowledge K. Altena-Schildkamp for N_2 chemisorption and CO/H_2 chemisorption measurements. The authors acknowledge T. Lubbers for XRF analysis.

Conflicts of Interests

The authors declare no conflict of interests.

Data Availability Statement

The data that support the findings of this study are available from the corresponding author upon reasonable request.

Keywords: Plasma-catalysis · ammonia · transition metals · kinetic analysis · Eley-Rideal reaction

[1] K. M. Van Geem, V. V. Galvita, G. B. Marin, *Science* **2019**, *364*, 734–73.

[2] P. Mehta, P. Barboun, D. B. Go, J. C. Hicks, W. F. Schneider, *ACS Energy Lett.* **2019**, *4*, 1115–1133.
[3] A. Bogaerts, E. C. Neyts, *ACS Energy Lett.* **2018**, *3*, 1013–1027.
[4] E. C. Neyts, K. Ostrikov, M. K. Sunkara, A. Bogaerts, *Chem. Rev.* **2015**, *115*, 13408–13446.
[5] H.-H. Kim, Y. Teramoto, A. Ogata, H. Takagi, T. Nanba, *Plasma Chem. Plasma Process.* **2016**, *36*, 45–72.
[6] E. C. Neyts, *Plasma Chem. Plasma Process.* **2016**, *36*, 185–212.
[7] A. Bogaerts, X. Tu, J. C. Whitehead, G. Centi, L. Lefferts, O. Guaitella, F. Azolina-Jury, H.-H. Kim, A. B. Murphy, W. F. Schneider, T. Nozaki, J. C. Hicks, A. Rousseau, F. Thevenet, A. Khacef, M. Carreon, *J. Phys. D* **2020**, *53*, 1–51.
[8] L. Ye, R. Nayak-Luke, R. Bañares-Alcántara, E. Tsang, *Chem* **2017**, *3*, 712–714.
[9] K. H. R. Rouwenhorst, A. G. J. Van Der Ham, G. Mul, S. R. A. Kersten, *Renewable Sustainable Energy Rev.* **2019**, *114*, 109339.
[10] K. H. R. Rouwenhorst, L. Lefferts, *Catalysts* **2020**, *10*, 999.
[11] IRENA, Ammonia Energy Association, *Innovation Outlook: Renewable Ammonia*, Abu Dhabi, **2022**.
[12] K. H. R. Rouwenhorst, Y. Engelmann, K. Van't Veer, R. S. Postma, A. Bogaerts, L. Lefferts, *Green Chem.* **2020**, *22*, 6258–6287.
[13] P. Peng, P. Chen, C. Schiappacasse, N. Zhou, E. Anderson, D. Chen, J. Liu, Y. Cheng, R. Hatzenbeller, M. Addy, Y. Zhang, Y. Liu, R. Ruan, *J. Cleaner Prod.* **2018**, *177*, 597–609.
[14] M. L. Carreon, *J. Phys. D* **2019**, *52*, 483001.
[15] J. Hong, S. Prawer, A. B. Murphy, *ACS Sustainable Chem. Eng.* **2018**, *6*, 15–31.
[16] L. R. Winter, J. G. Chen, *Joule* **2021**, *17*, 1–16.
[17] A. Bogaerts, X. Tu, J. C. Whitehead, G. Centi, L. Lefferts, O. Guaitella, F. Azolina-Jury, H.-H. Kim, A. B. Murphy, W. F. Schneider, T. Nozaki, J. C. Hicks, A. Rousseau, F. Thevenet, A. Khacef, M. Carreon, *J. Phys. D* **2020**, *53*, 1–51.
[18] P. Mehta, P. Barboun, F. A. Herrera, J. Kim, P. Rumbach, D. B. Go, J. C. Hicks, W. F. Schneider, *Nat. Catal.* **2018**, *1*, 269–275.
[19] P. Mehta, P. Barboun, Y. Engelmann, D. B. Go, A. Bogaerts, W. F. Schneider, J. C. Hicks, *ACS Catal.* **2020**, *10*, 6726–6734.
[20] S. Dahl, A. Logadottir, C. J. H. Jacobsen, J. K. Norskov, *Appl. Catal. A* **2001**, *222*, 19–29.
[21] K. H. R. Rouwenhorst, L. Lefferts, *J. Phys. D* **2021**, *54*, 393002.
[22] K. H. R. Rouwenhorst, H.-H. Kim, L. Lefferts, *ACS Sustainable Chem. Eng.* **2019**, *7*, 17515–17522.
[23] Z. Chen, B. E. Koel, S. Sundaresan, *J. Phys. D* **2022**, *55*, 055202.
[24] Y. Engelmann, K. van't Veer, Y. Gorbanev, E. C. Neyts, W. F. Schneider, A. Bogaerts, *ACS Sustainable Chem. Eng.* **2021**, *9*, 13151–13163.
[25] Y. Gorbanev, Y. Engelmann, K. Van't Veer, E. Vlasov, C. Ndayirinde, Y. Yi, S. Bals, A. Bogaerts, *Catalysts* **2021**, *11*, 1230.
[26] K. H. R. Rouwenhorst, H. G. B. Burbach, J. Núñez Paulí, D. W. Vogel, B. Geerdink, L. Lefferts, *Catal. Sci. Technol.* **2021**, *11*, 2834–2843.
[27] J. Shah, W. Wang, A. Bogaerts, M. L. Carreon, *ACS Appl. Energ. Mater.* **2018**, *1*, 4824–4839.
[28] S. S. R. K. C. Yamijala, G. Nava, Z. A. Ali, D. Beretta, B. M. Wong, L. Mangolini, *J. Phys. Chem. Lett.* **2020**, *11*, 10469–10475.
[29] K. H. R. Rouwenhorst, H. G. B. Burbach, J. Núñez Paulí, D. W. Vogel, B. Geerdink, L. Lefferts, *Catal. Sci. Technol.* **2021**, *11*, 2834–2843.
[30] Y. Engelmann, K. van't Veer, Y. Gorbanev, E. C. Neyts, W. F. Schneider, A. Bogaerts *ACS Sustainable Chem. Eng.* **2021**, *9*, 13151–13163.
[31] B. S. Patil, N. Cherkasov, N. V. Srinath, J. Lang, A. O. Ibhadon, Q. Wang, V. Hessel, *Catal. Today* **2020**, *362*, 2–10.
[32] P. M. Barboun, P. Mehta, F. Herrera, D. B. Go, W. F. Schneider, J. C. Hicks, *ACS Sustainable Chem. Eng.* **2019**, *7*, 8621–8630.
[33] M. Iwamoto, M. Akiyama, K. Aihara, T. Deguchi, *ACS Catal.* **2017**, *7*, 6924–6929.
[34] M. Iwamoto, M. Horikoshi, R. Hashimoto, K. Shimano, T. Sawaguchi, H. Teduka, M. Matsukata, *Catalysts* **2020**, *10*, 590.
[35] Y. Wang, M. Craven, X. Yu, J. Ding, P. Bryant, J. Huang, X. Tu, *ACS Catal.* **2019**, *9*, 10780–10793.
[36] Z. Chen, B. E. Koel, S. Sundaresan, *J. Phys. D* **2022**, *55*, 055202.
[37] Y. Gorbanev, Y. Engelmann, K. Van't Veer, E. Vlasov, C. Ndayirinde, Y. Yi, S. Bals, A. Bogaerts, *Catalysts* **2021**, *11*, 1230.
[38] H. Zhao, G. Song, Z. Chen, X. Yang, C. Yan, S. Abe, Y. Ju, S. Sundaresan, B. E. Koel, *ACS Energy Lett.* **2022**, *7*, 53–58.
[39] P. M. Barboun, P. Mehta, F. Herrera, D. B. Go, W. F. Schneider, J. C. Hicks, *ACS Sustainable Chem. Eng.* **2019**, *7*, 8621–8630.
[40] P. Mehta, P. Barboun, Y. Engelmann, D. B. Go, A. Bogaerts, W. F. Schneider, J. C. Hicks, *ACS Catal.* **2020**, *10*, 6726–6734.
[41] J. C. Ganley, F. S. Thomas, E. G. Seebauer, R. I. Masel, *Catal. Lett.* **2004**, *96*, 117–122.
[42] T. E. Bell, L. Torrente-Murciano, *Top. Catal.* **2016**, *59*, 1438–1457.
[43] K. W. Frese, *Surf. Sci.* **1987**, *182*, 85–97.
[44] H. Falsig, J. Shen, T. S. Khan, W. Guo, G. Jones, S. Dahl, T. Bligaard, *Top. Catal.* **2014**, *57*, 80–88.
[45] S. Wang, V. Petzold, V. Tripkovic, J. Kleis, J. G. Howalt, E. Skúlason, E. M. Fernández, B. Hvolbæk, G. Jones, A. Toftelund, H. Falsig, M. Björketun, F. Studt, F. Abild-Pedersen, J. Rossmeisl, J. K. Nørskov, T. Bligaard, *J. Phys. D* **2011**, *13*, 20760–20765.
[46] K. H. R. Rouwenhorst, L. Lefferts, *J. Phys. D* **2021**, *54*, 393002.
[47] H. Liu, *Ammonia Synthesis Catalysts: Innovation and Practice*, World Scientific, China, **2013**.
[48] A. Bogaerts, Q.-Z. Zhang, Y.-R. Zhang, K. Van Laer, W. Wang, *Catal. Today* **2019**, *337*, 3–14.
[49] F. A. Herrera, G. H. Brown, P. Barboun, N. Turan, P. Mehta, W. F. Schneider, J. C. Hicks, D. B. Go, *J. Phys. D* **2019**, *52*, 224002.
[50] L. R. Ventura, C. E. Fellows, *J. Quant. Spectrosc. Radiat. Transfer* **2019**, *239*, 106645.
[51] P. Navascués, J. M. Obrero-Pérez, J. Cotrino, A. R. González-Elipe, A. Gómez-Ramírez, *Catalysts* **2019**, *9*, 45.
[52] P. Navascués, J. M. Obrero-Pérez, J. Cotrino, A. R. González-Elipe, A. Gómez-Ramírez, *ACS Sustainable Chem. Eng.* **2020**, *8*, 14855–14866.
[53] K. Van't Veer, Y. Engelmann, F. Reniers, A. Bogaerts, *J. Phys. Chem. C* **2020**, *124*, 22871–22883.
[54] A. Jess, P. Wasserscheid, *Chemical Technology: An Integral Textbook*, Wiley-VCH, Weinheim **2013**.

Manuscript received: January 23, 2023
Revised manuscript received: March 28, 2023
Accepted manuscript online: April 3, 2023
Version of record online: May 15, 2023